

# Monolayer excitonic laser

Yu Ye<sup>1,2†</sup>, Zi Jing Wong<sup>1,2†</sup>, Xiufang Lu<sup>3</sup>, Xingjie Ni<sup>1,2</sup>, Hanyu Zhu<sup>1</sup>, Xianhui Chen<sup>3</sup>, Yuan Wang<sup>1,2</sup> and Xiang Zhang<sup>1,2,4\*</sup>

**Two-dimensional van der Waals materials have opened a new paradigm for fundamental physics exploration and device applications because of their emerging physical properties. Unlike gapless graphene, monolayer transition-metal dichalcogenides (TMDCs) are two-dimensional semiconductors that undergo an indirect-to-direct bandgap transition<sup>1–5</sup>, creating new optical functionalities for next-generation ultra-compact photonics and optoelectronics. Although the enhancement of spontaneous emission has been reported on TMDC monolayers integrated with photonic crystals<sup>6,7</sup> and distributed Bragg reflector microcavities<sup>8,9</sup>, coherent light emission from a TMDC monolayer has not been demonstrated. Here, we report the realization of a two-dimensional excitonic laser by embedding monolayer WS<sub>2</sub> in a microdisk resonator. Using a whispering gallery mode with a high quality factor and optical confinement, we observe bright excitonic lasing at visible wavelengths. This demonstration of a two-dimensional excitonic laser marks a major step towards two-dimensional on-chip optoelectronics for high-performance optical communication and computing applications.**

As a direct bandgap semiconductor, transition-metal dichalcogenide (TMDC) monolayers have attracted increasing attention for electronic and optoelectronic applications due to their strong light emission accompanied with unique access to spin and valley degrees of freedom<sup>10–13</sup>. These properties arise from the quantum confinement and crystal symmetry effect on the electronic band structure as the material is thinned down to a monolayer configuration. The demonstrations of excellent on-off ratio transistors<sup>14</sup>, valley-Hall physics<sup>15</sup>, large exciton binding energy<sup>16–18</sup>, light-emitting diodes<sup>3–5</sup>, superconductivity<sup>19</sup>, sensors<sup>20</sup> and piezoelectricity<sup>21,22</sup> show the diverse physics and applications of this material system. However, coherent light emission, or lasing, an essential step towards the realization of on-chip photonic applications, has not been realized. The design and fabrication of microcavities is crucial for a two-dimensional laser, which requires a high optical mode confinement factor and high quality factor Q. Here, we demonstrate a two-dimensional excitonic laser using monolayer WS<sub>2</sub> coupled to a microdisk resonator, which has high quantum yield, small footprint and low power consumption.

TMDCs such as WS<sub>2</sub> (Fig. 1a) evolve from indirect- to direct-bandgap semiconductors as the number of layers is reduced from bulk to monolayer, with sizable bandgaps around 2.0 eV at visible wavelengths. The direct bandgaps sit at the K and K' valleys (Fig. 1b), two non-equivalent momentum valleys in the reciprocal space of the monolayer WS<sub>2</sub> protected by the crystal's broken inversion symmetry, providing rich valley-contrasting physics<sup>10–13</sup>. The transition between valence band and conduction band-edge is excitonic in nature in such a monolayer system. Strong excitonic features, including neutral and redshifted charged excitons, have

been observed and studied<sup>23</sup>. The exciton in two-dimensional TMDCs not only governs the emissions properties, but also allows for the long-lived population inversion required to achieve optical gain and possible stimulated emissions. Although Purcell enhancement of spontaneous emission has been achieved in photonic crystals and distributed Bragg reflector microcavities<sup>6–9</sup>, coherent light emission or lasing from a two-dimensional semiconducting TMDC has not been demonstrated due to the limited material gain volume, and the lack of optical confinement and feedback within the atomic monolayer.

Here, we report a monolayer excitonic laser in a microdisk resonator (Fig. 1c). By integrating the monolayer WS<sub>2</sub> into a strong-feedback photonic cavity, the build-up of stimulated emission can eventually exceed the lasing threshold. Microdisks feature low-loss, high-quality whispering gallery modes (WGMs) that offer the potential for ultralow-threshold lasing<sup>24</sup>. Embedding the monolayer between two dielectric layers (Si<sub>3</sub>N<sub>4</sub>/WS<sub>2</sub>/hydrogen silsesquioxane (HSQ)) enables strong optical confinement and leads to a larger modal gain, necessary for an atomically thin monolayer gain medium. The scanning electron microscope (SEM) image in Fig. 1d of the undercut Si<sub>3</sub>N<sub>4</sub>/WS<sub>2</sub>/HSQ microdisk shows the low sidewall roughness that is essential to obtain a high cavity Q. The diameter of the HSQ layer is slightly smaller than that of the Si<sub>3</sub>N<sub>4</sub> layer due to the finite etching selectivity between the HSQ and Si<sub>3</sub>N<sub>4</sub>.

The cavity resonance is designed to overlap with the gain spectrum of monolayer WS<sub>2</sub> (Supplementary Section Ib), with the electric field polarized in the plane of the TMDC monolayer to efficiently couple with the in-plane dipoles of the excitons<sup>25</sup>. For a Si<sub>3</sub>N<sub>4</sub>/HSQ microdisk structure with a diameter of 3.3 μm, we expect a strong transverse electric (TE)-polarized WGM at a wavelength of 612 nm. The small diameter of the microdisk ensures other resonance modes are widely separated in wavelength to avoid mode competition. Reducing the number of modes will also increase the spontaneous emission factor and contribute to the improvement of the lasing threshold. The electric field distribution of the TE<sub>1,24</sub> resonance (radial mode number  $l=1$ , azimuthal mode number  $m=24$ ) is shown in Fig. 2a (top view) and Fig. 2b (cross-sectional view). The resonant wavelength matches the dominant peak of the measured lasing spectrum from a WS<sub>2</sub> monolayer embedded within a 3.3-μm-diameter microdisk at 612.2 nm (Fig. 2c), with a measured  $Q=\lambda/\Delta\lambda$  of ~2,604. The sandwiched configuration provides two advantages: (1) enhanced optical mode overlap, (2) material protection. It is important to note that the optical confinement factor of our Si<sub>3</sub>N<sub>4</sub>/WS<sub>2</sub>/HSQ structure is ~30% higher than in the case where the monolayer is directly transferred onto the top of a pre-built microdisk (Supplementary Section Ic). The enhanced confinement factor is one order larger than those of low-threshold quantum-dot microdisk lasers<sup>26</sup>. It is worth

<sup>1</sup>NSF Nanoscale Science and Engineering Center, University of California, Berkeley, California 94720, USA. <sup>2</sup>Materials Sciences Division, Lawrence Berkeley National Laboratory, Berkeley, California 94720, USA. <sup>3</sup>Hefei National Laboratory for Physical Science at Microscale and Department of Physics, University of Science and Technology of China, Hefei, Anhui 230026, China. <sup>4</sup>Department of Physics, King Abdulaziz University, Jeddah 21589, Saudi Arabia;

\*These authors contributed equally to this work. \*e-mail: [xiang@berkeley.edu](mailto:xiang@berkeley.edu)

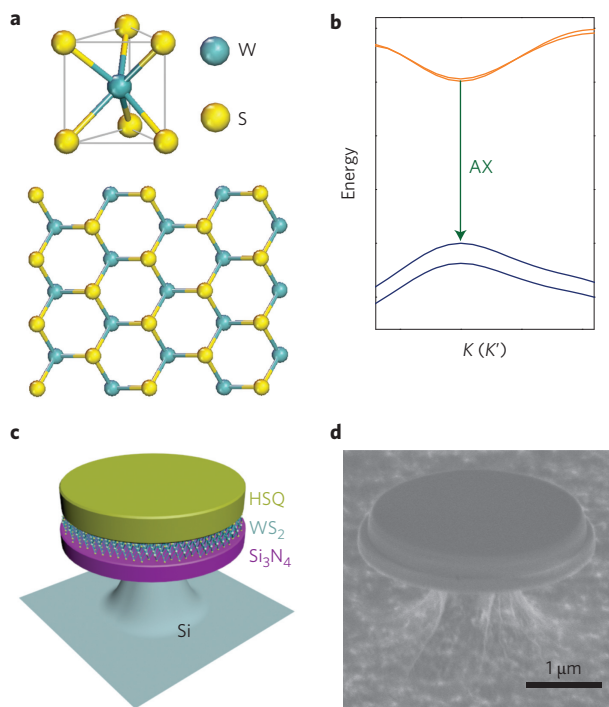


**Figure 1 | Design of the monolayer exitonic laser.** **a**, A single layer of WS<sub>2</sub> comprising S–W–S stacking, with a total thickness of 0.65 nm. In the top view, each unit cell can be seen to consist of two S atoms occupying the same site in the hexagonal lattice, with the W atom residing at the opposite site. **b**, Band structure at the  $K$  ( $K'$ ) point, showing the direct band A exciton (AX) transition, and valence band splitting due to spin-orbit coupling. **c**, Schematic image of a monolayer WS<sub>2</sub> microdisk laser. The sandwich structure, Si<sub>3</sub>N<sub>4</sub>/WS<sub>2</sub>/HSQ, ensures a higher confinement factor and leads to a larger modal gain. **d**, SEM of an undercut Si<sub>3</sub>N<sub>4</sub>/WS<sub>2</sub>/HSQ microdisk, showing the smooth sidewall essential for achieving a high cavity quality factor.

mentioning that the lasing performance of our two-dimensional laser does not decay even after one year, as our sandwiched structure protects the monolayer from direct exposure to air, which is known to degrade its luminescence property<sup>27</sup>. In addition, the whispering gallery resonance feature of our structure is further verified by the three additional peaks in the photoluminescence spectrum, that is, at 633.7 nm, 657.6 nm and 683.7 nm, corresponding to the TE<sub>1,23</sub>, TE<sub>1,22</sub> and TE<sub>1,21</sub> modes in simulation (Supplementary Section Ib). Such modes are only observed on the low-energy side of the spectrum, as high-energy photons are more likely to be reabsorbed before coupling to the cavity resonance<sup>24</sup>.

To study the emission characteristics of the monolayer WS<sub>2</sub> microdisk laser, the device was optically pumped with an ultrafast laser (190 fs pulse duration, 80 MHz repetition rate) at 473 nm and 10 K. The pump source was switched on only for 190 fs time intervals, which are short enough to significantly minimize heating and all related thermal effects, allowing operation at higher peak power densities above lasing threshold. The device has a diameter of 3.3  $\mu$ m and the emission spectra were collected ( $\times 50$ , objective of 0.55 NA) as a function of pump intensity (Fig. 3a). At the lowest pump intensity we observe a broad emission corresponding to the photoluminescence of the WS<sub>2</sub>. For pump intensities between 3.14 MW cm<sup>-2</sup> and 22.4 MW cm<sup>-2</sup>, a shoulder appears at 612.2 nm, amplified by the optical feedback in the micro-disk cavity. Above 22.4 MW cm<sup>-2</sup>, the peak increases sharply in intensity, showing clear evidence of lasing. In an atomically thin TMDC monolayer, the optical transition spectrum in the non-interacting limit exhibits a step-like function. The strong confinement enhances the electron–hole interaction, leading to a large binding

energy and sharp excitonic levels<sup>16–18,23</sup>, which further increases the optical gain and narrows the gain spectrum compared with those in the non-interacting limit. This modification of the optical transition oscillator strength is predicted to result in several improvements in the laser characteristics, such as a lower threshold, higher modulation bandwidth and smaller emission linewidth<sup>28</sup>. The 10 K photoluminescence spectrum at a pump intensity of 65.7 MW cm<sup>-2</sup> (Fig. 3b) is well fitted with bi-Lorentzian curves, where the peak intensity of both the broad monolayer WS<sub>2</sub> photoluminescence spectrum background and narrow cavity emission are extracted. In Fig. 3c, the pump intensity dependence of the photoluminescence emission ( $L$ – $L$  curves) is plotted for both the cavity and the background photoluminescence emission. Below the lasing threshold, the cavity emission increases linearly with excitation energy. Above the threshold, a distinct kink is observed in the  $L$ – $L$  curve, with a superlinear increase in the emission output. In contrast, the monolayer WS<sub>2</sub> background photoluminescence emission maintains a linear dependence on all pump energies because the emission is mainly from the centre of the microdisk and does not couple to the cavity mode. In WGMs, electric fields are mainly localized at the edges of the microdisk. The electrical field distribution for the lasing mode (612.2 nm) and non-lasing mode (633.7 nm) heavily overlap one another, indicating their competitive nature in terms of carrier depletion. Compared with the WS<sub>2</sub> lasing mode (612.2 nm), the 633.7 nm WGM (Fig. 3d) does not show any lasing behaviour due to the insufficient optical gain at a wavelength off the resonance of the excitonic transition in monolayer WS<sub>2</sub>. Under lasing conditions, the 633.7 nm WGM emission clamps after the lasing threshold, because the pump power is converted to the cavity lasing photon population. The clamping of the competing non-lasing modes beyond the lasing threshold is well studied as an experimental signature of lasing<sup>29</sup>. The lasing behaviour was also observed in another monolayer WS<sub>2</sub> laser (Supplementary Section IV) with high  $Q$ , indicating the high repeatability of this arrangement.

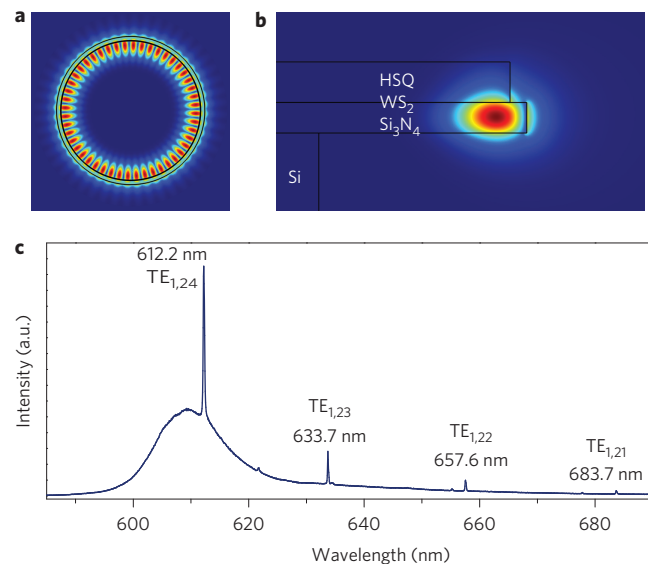


**Figure 2 | Whispering gallery modes of the monolayer exitonic laser.** **a**, Top view of the simulated electric field distribution of the TE<sub>1,24</sub> resonance. **b**, Cross-sectional view of the calculated electric field distribution of the TE<sub>1,24</sub> resonance. The Si<sub>3</sub>N<sub>4</sub>/WS<sub>2</sub>/HSQ sandwich structure enhances the optical mode overlap with monolayer WS<sub>2</sub>. Red and blue colours corresponds to the maximum and minimum of the field density, respectively. The boxed outlines refer to the structure boundary. **c**, Experimental photoluminescence spectrum taken at 10 K when the pump intensity is above lasing threshold, showing WGMs at 612.2 nm, 633.7 nm, 657.6 nm and 683.7 nm.

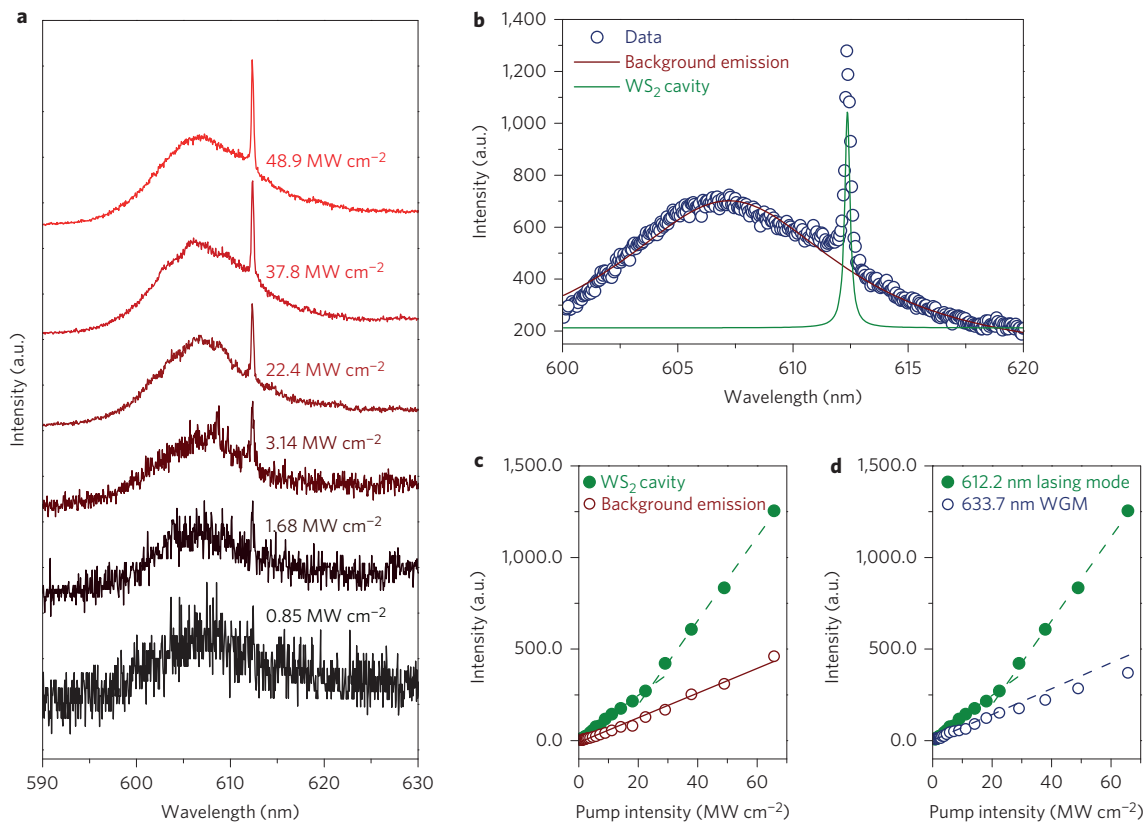


**Figure 3 | Observation of monolayer WS<sub>2</sub> excitonic lasing.** **a**, Steady-state photoluminescence emission spectra with increasing pump intensity, normalized to pump intensity, illustrating the transition from spontaneous emission to stimulated emission and lasing. **b**, Photoluminescence spectrum for a pump intensity of 65.7 MW cm<sup>-2</sup>. Symbols show the measured data, the brown line is a fit to the monolayer WS<sub>2</sub> photoluminescence background emission (from the centre of the microdisk), and the green line is a fit to the WS<sub>2</sub> cavity emission. **c**, Monolayer WS<sub>2</sub> photoluminescence background and cavity emissions as a function of pump intensity. Dashed lines represent linear fits to the experimental data. The WS<sub>2</sub> photoluminescence background emission shows a linear dependence on the pump intensity, and the green dashed lines (cavity emission) show a kink indicating the onset of superlinear emission and lasing operation. **d**, WGM emission (633.7 nm) clamps after the lasing threshold.

To further verify the lasing behaviour, the emission from our device was integrated for 5 s to carefully resolve the evolution of the extremely narrow spectral linewidth as the pump intensity was gradually increased beyond the lasing threshold. Using a rate equation analysis, we found the lasing threshold to be around 5–8 MW cm<sup>-2</sup> pump intensity, with an extracted average threshold modal gain of 78.8 cm<sup>-1</sup> for the best fitted spontaneous emission factor  $\beta$  of 0.5 (Fig. 4a). Due to the high  $Q$  of our cavity, the Purcell effect significantly enhances the spontaneous emission factor  $\beta$ , where more spontaneous emission is now directly coupled to the desired lasing mode. Coupled with the larger  $\beta$  factor, the transition kink between the spontaneous emission regime and the stimulated emission smears, leading to a soft lasing threshold of ~5–8 MW cm<sup>-2</sup> (Supplementary Sections III and V).  $L$ - $L$  curves for values of  $\beta$  of 0.005, 0.05 and 1 are also presented for comparison.

High-resolution spectra of WS<sub>2</sub> cavity mode emission at spontaneous emission (4.9 MW cm<sup>-2</sup>) and the laser oscillation regime (92.1 MW cm<sup>-2</sup>) are also presented. In the spontaneous emission regime (Fig. 4c), the full-width at half-maximum (FWHM) of the mode emission is 0.28 nm and reduces to 0.24 nm when the excitation intensity reaches the laser oscillation regime (Fig. 4d), clearly showing the linewidth narrowing effect (Fig. 4b) observed in standard lasers. The small linewidth narrowing at the threshold is typical for high  $\beta$  factor lasers<sup>30–33</sup>. We found that a high  $Q$  is necessary to achieve lasing oscillation in our monolayer WS<sub>2</sub> micro-disk. A lower cavity  $Q$  of ~1,162, measured in another sample, prevents lasing due to the significant resonator losses.

The internal luminescence quantum yield, defined by the fraction of absorbed photons that emit radiatively, is one of the key elements necessary for a laser. A high quantum yield is crucial to achieve a large optical gain, leading to a lower threshold pump power. The quantum yields of different TMDC monolayers may vary widely due to unintentional doping during the synthetic/natural growth process of the crystals. We experimentally measured the photoluminescence of MoS<sub>2</sub>, WS<sub>2</sub> and WSe<sub>2</sub> monolayers, and quantified their respective quantum yields to determine the optimal monolayer TMDC material for lasing applications. The monolayer quantum yield was extracted by measuring the absorption (in addition to photoluminescence), and calibrated using standard rhodamine 6G samples as the control<sup>1,34</sup> (Supplementary Section Ia). The monolayer WS<sub>2</sub> at cryogenic temperatures was found to have the largest quantum yield (~6%), five times and two orders larger than the quantum yields of monolayer WSe<sub>2</sub> and MoS<sub>2</sub>, respectively, making it our optimal TMDC of choice for optical gain.

In summary, we have demonstrated visible emission from a two-dimensional excitonic laser using monolayer WS<sub>2</sub> as a novel gain medium. The ability to generate coherent light radiation in an atomically thin semiconducting monolayer paves the way for two-dimensional coherent control and van der Waals-based optoelectronics. Selective excitation of the carrier population in one set of two distinct valleys can further lead to lasing in the confined valley, a key element for future valley optoelectronics.

*Note added in proof:* While this manuscript was under review, two related works were reported<sup>35,36</sup>.

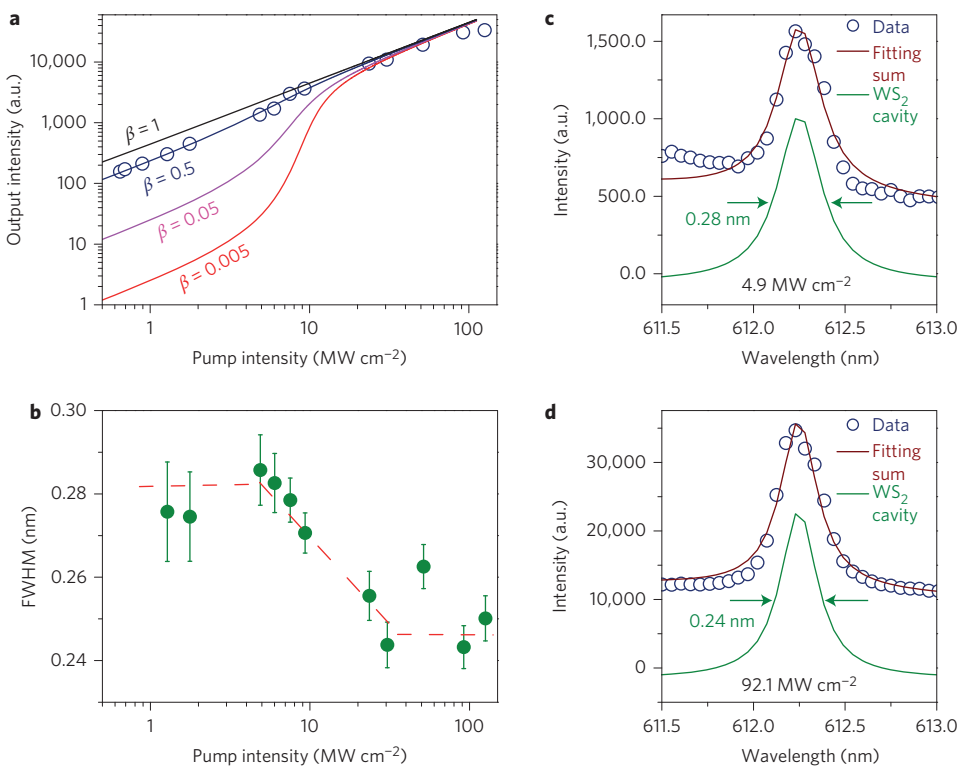


**Figure 4 | Characterizations of two-dimensional excitonic lasing.** **a**, Experimental data and rate equation analytical fits. The best fit to the experimental data gives a threshold pump intensity of  $\sim 5\text{--}8 \text{ MW cm}^{-2}$  with a spontaneous emission factor,  $\beta$ , of 0.5. The fits to  $\beta$  of 0.005, 0.05 and 1 are also presented for comparison. **b**, FWHM versus input pump intensity. Linewidth narrowing of the lasing mode is observed as the excitation intensity exceeds the lasing threshold. The red dashed line is a guide to the eye. The linewidth error bar is too large at low pump intensity to determine the real linewidth. **c**, High-resolution spectrum in the spontaneous emission regime ( $4.9 \text{ MW cm}^{-2}$ ). The cavity emission (green curve) gives a FWHM of 0.28 nm. **d**, High-resolution spectrum in the lasing oscillator regime ( $92.1 \text{ MW cm}^{-2}$ ). The cavity emission (green curve) gives a FWHM of 0.24 nm.

Received 6 February 2015; accepted 17 September 2015;  
published online 19 October 2015

## References

- Mak, K. F., Lee, C., Hone, J., Shan, J. & Heinz, T. F. Atomically thin MoS<sub>2</sub>: a new direct-gap semiconductor. *Phys. Rev. Lett.* **105**, 136805 (2010).
- Splendiani, A. *et al.* Emerging photoluminescence in monolayer MoS<sub>2</sub>. *Nano Lett.* **10**, 1271–1275 (2010).
- Ross, J. S. *et al.* Electrically tunable excitonic light-emitting diodes based on monolayer WSe<sub>2</sub> p-n junctions. *Nature Nanotech.* **9**, 268–272 (2014).
- Pospischil, A., Furchi, M. M. & Mueller, T. Solar-energy conversion and light emission in an atomic monolayer p-n diode. *Nature Nanotech.* **9**, 257–261 (2014).
- Baugher, B. W. H., Churchill, H. O. H., Yang, Y. & Jarillo-Herrero, P. Optoelectronic devices based on electrically tunable p-n diodes in a monolayer dichalcogenide. *Nature Nanotech.* **9**, 262–267 (2014).
- Wu, S. *et al.* Control of two-dimensional excitonic light emission via photonic crystal. *2D Mater.* **1**, 011001 (2014).
- Gan, X. *et al.* Controlling the spontaneous emission rate of monolayer MoS<sub>2</sub> in a photonic crystal nanocavity. *Appl. Phys. Lett.* **103**, 18119 (2013).
- Liu, X. *et al.* Strong light-matter coupling in two-dimensional atomic crystals. *Nature Photon.* **9**, 30–34 (2015).
- Schwarz, S. *et al.* Two-dimensional metal-chalcogenide films in tunable optical microcavities. *Nano Lett.* **14**, 7003–7008 (2014).
- Mak, K. F., He, K., Shan, J. & Heinz, T. F. Control of valley polarization in monolayer MoS<sub>2</sub> by optical helicity. *Nature Nanotech.* **7**, 494–498 (2012).
- Cao, T. *et al.* Valley-selective circular dichroism of monolayer molybdenum disulfide. *Nature Commun.* **3**, 887 (2012).
- Zeng, H., Dai, J., Yao, W., Xiao, D. & Cui, X. Valley polarization in MoS<sub>2</sub> monolayer by optical pumping. *Nature Nanotech.* **7**, 490–493 (2012).
- Xiao, D., Liu, G., Feng, W., Xu, X. & Yao, W. Coupled spin and valley physics in monolayer of MoS<sub>2</sub> and other group-VI dichalcogenides. *Phys. Rev. Lett.* **108**, 196802 (2012).
- Radisavljevic, B., Radenovic, A., Brivio, J., Giacometti, V. & Kis, A. Single-layer MoS<sub>2</sub> transistors. *Nature Nanotech.* **6**, 147–150 (2011).
- Mak, K. F., McGill, K. L., Park, J. & McEuen, P. L. The valley Hall effect in MoS<sub>2</sub> transistors. *Science* **344**, 1489–1492 (2014).
- Chernikov, A. *et al.* Exciton binding energy and nonhydrogenic Rydberg series in monolayer WSe<sub>2</sub>. *Phys. Rev. Lett.* **113**, 076802 (2014).
- He, K. *et al.* Tightly bound excitons in monolayer WSe<sub>2</sub>. *Phys. Rev. Lett.* **113**, 026803 (2014).
- Ye, Z. *et al.* Probing excitonic dark states in single-layer tungsten disulfide. *Nature* **513**, 214–218 (2014).
- Ye, J. T. *et al.* Superconducting dome in a gate-tuned band insulator. *Science* **338**, 1193–1196 (2012).
- Perkins, F. K. *et al.* Chemical vapor sensing with monolayer MoS<sub>2</sub>. *Nano Lett.* **13**, 668–673 (2013).
- Wu, W. *et al.* Piezoelectricity of single-atomic-layer MoS<sub>2</sub> for energy conversion and piezotronics. *Nature* **514**, 470–474 (2014).
- Zhu, H. *et al.* Observation of piezoelectricity in free-standing monolayer MoS<sub>2</sub>. *Nature Nanotech.* **10**, 151–155 (2015).
- Mak, K. F. *et al.* Tightly bound trions in monolayer MoS<sub>2</sub>. *Nature Mater.* **12**, 207–211 (2013).
- Tamboli, A. C. *et al.* Room-temperature continuous-wave lasing in GaN/InGaN microdisks. *Nature Photon.* **1**, 61–64 (2007).
- Schuller, J. A. *et al.* Orientation of luminescent excitons in layered nanomaterials. *Nature Nanotech.* **8**, 271–276 (2013).
- Bimberg, D. *et al.* InGaAs–GaAs quantum-dot lasers. *IEEE J. Sel. Topics Quantum Electron.* **3**, 196–205 (1997).
- Zhao, W. *et al.* Evolution of electronic structure in atomically thin sheets of WS<sub>2</sub> and WSe<sub>2</sub>. *ACS Nano* **7**, 791–797 (2013).
- Arakawa, Y. & Yariv, A. Quantum well lasers—gain, spectra, dynamics. *IEEE J. Sel. Topics Quantum Electron.* **22**, 1887–1899 (1986).
- Hendrickson, J. *et al.* Quantum dot photonic-crystal-slab nanocavities: quality factors and lasing. *Phys. Rev. B* **72**, 193303 (2005).
- Hsu, K. S. *et al.* Compact microdisk cavity laser with type-II GaSb/GaAs quantum dots. *Appl. Phys. Lett.* **98**, 051105 (2011).
- Eichfelder, M. *et al.* Room-temperature lasing of electrically pumped red-emitting InP/(Al<sub>0.20</sub>Ga<sub>0.80</sub>)<sub>0.51</sub>In<sub>0.49</sub>P quantum dots embedded in vertical microcavity. *Appl. Phys. Lett.* **95**, 131107 (2009).

32. Gong, Y. *et al.* Nanobeam photonic crystal cavity quantum dot laser. *Opt. Express* **18**, 8781–8789 (2010).
33. Mohideen, U. & Slusher, R. E. Semiconductor microlaser linewidths. *Phys. Rev. Lett.* **73**, 1785–1788 (1994).
34. Ammer, F., Penzkofer, A. & Weidner, P. Concentration-dependent fluorescence behavior of oxazine 750 and rhodamine 6G in porous silicate xerogel monoliths. *Chem. Phys.* **192**, 325–331 (1995).
35. Wu, S. *et al.* Monolayer semiconductor nanocavity with ultralow thresholds. *Nature* **520**, 69–72 (2015).
36. Salehzadeh, O., Djavid, M., Tran, N. H., Shih, I. & Mi, Z. Optically pumped two-dimensional MoS<sub>2</sub> lasers operating at room-temperature. *Nano Lett.* **15**, 5302–5306 (2015).

### Acknowledgements

The authors acknowledge financial support from the US Air Force Office of Scientific Research under award no. FA9550-12-1-0197 (Optical Design and Characterization), and the ‘Light–Material Interaction in Energy Conversion’ Energy Frontier Research Center funded by the US Department of Energy, Office of Science, Office of Basic Energy Sciences

under award no. DE-AC02-05CH11231 (Materials Synthesis and Lithography). The authors also thank A. Grine for his help in measuring the passive Q factor of the cavity.

### Author contributions

X.Z., Y.W., Y.Y. and Z.J.W. conceived the project. X.L. and X.C. grew bulk WS<sub>2</sub> crystals. Y.Y., Z.J.W. and H.Z. developed the sample design and fabricated the samples. Y.Y., Z.J.W. and X.N. performed the measurements. Z.J.W. and Y.Y. performed the numerical simulation. Y.Y. and Z.J.W. carried out the data analysis. Y.Y., Z.J.W., X.Z. and Y.W. wrote the manuscript. X.Z. and Y.W. guided the research. All authors contributed to discussions.

### Additional information

Supplementary information is available in the online version of the paper. Reprints and permissions information is available online at [www.nature.com/reprints](http://www.nature.com/reprints). Correspondence and requests for materials should be addressed to X.Z.

### Competing financial interests

The authors declare no competing financial interests.